Full Paper Transactions, SMiRT 28
Toronto, Canada, August 10-15, 2025

EXPERIMENTAL VERIFICATION OF A SMOOTH DAMPING CONTROL STRATEGY FOR A SEMI-ACTIVE ELECTROMAGNETIC SEISMIC ISOLATION SYSTEM

Ging-Long Lin[1], Tse-Chi Chen[2], Chi-Chang Lin[3]

[1] Associate Professor, National Kaohsiung University of Science and Technology, Kaohsiung, Taiwan. (gllin@nkust.edu.tw)
[2] Graduated Student, National Kaohsiung University of Science and Technology, Kaohsiung, Taiwan. (pppppppppp31@gmail.com)
[3]Honorary Distinguished Professor, National Chung Hsing University, Taichung, Taiwan. (cclin3@dragon.nchu.edu.tw)

ABSTRACT

Passive seismic isolation systems with fixed damping ratios struggle to balance isolation demands for near-fault and far-field seismic excitations. Under far-field earthquakes, passive isolation systems effectively reduce the absolute acceleration response of the isolated structure, demonstrating superior isolation performance. However, when subjected to near-fault earthquakes, passive systems may experience excessive isolation displacements. To address this issue, this study develops a Semi-Active Electromagnetic Seismic Isolation System (SA-EMSIS), which uses the relative velocity of the isolation layer with respect to the ground as the feedback signal. A hyperbolic tangent function (*tanh*) function is employed as the controller to smoothly and continuously adjust the damping ratio of the SA-EMSIS. Shaking table test results show good agreement between theoretical analysis and experimental outcomes, verifying the accuracy of the theoretical model and the reliability of the experimental setup. Compared to passive isolation systems, the SA-EMSIS with the *tanh* controller significantly reduces isolation displacement under near-fault seismic excitations without amplifying isolation acceleration under far-field seismic excitations, achieving more comprehensive isolation performance. Owing to its real-time damping adjustability, the SA-EMSIS shows promise for protecting critical equipment in nuclear facilities.

INTRODUCTION

Traditional seismic isolation techniques have been widely acknowledged and extensively applied (Naeim and Kelly (1999)). However, studies have shown that the long-period velocity pulses characteristic of near-fault ground motions may resonate with the natural period of isolation systems (He and Agrawal (2008); Makris and Vassiliou (2011)), leading to excessive isolation displacement. While increasing the damping ratio of the isolation system effectively suppresses displacement (Lu et al. (2013)), the optimal damping ratio for near-fault ground motions is significantly higher than that required for far-field ground motions. Under far-field seismic excitations, applying a higher damping ratio reduces isolation efficiency by increasing the acceleration response of the isolated structure. Therefore, isolation systems with fixed damping ratios cannot simultaneously meet the demands of both near-fault and far-field ground motions.

Electromagnetic dampers have gained attention for their dual functionality in vibration control and energy harvesting. Palomera-Arias (2005) compared the damping density and cost-effectiveness of electromagnetic and traditional viscous dampers, revealing that the cost of electromagnetic dampers is slightly higher than that of viscous dampers under identical maximum damping density. Given the dual capabilities of vibration reduction and power generation, researchers have focused on optimizing the efficiency of both functions (Tai and Zuo (2017); Sun et al. (2023)). Cai and Zhu (2019) and Li and Zhu (2021) further enhanced the power generation and self-sustaining capabilities of electromagnetic dampers.

To mitigate the adverse effects of near-fault ground motions on isolation systems, Lin et al. (2022) developed electromagnetic base isolation systems (EMSIS) to investigate the impact of electromagnetic damping on isolation performance. Subsequently, Lin et al. (2025a) incorporated a flywheel into EMSIS, creating the EMSIS-FW system, and studied the effects of replacing part of the isolation layer's mass with inertance on seismic isolation performance. Lin et al. (2025b) also developed a prototype of a semi-active electromagnetic seismic isolation system (SA-EMSIS) and verified the controllability of isolation layer damping through shaking table tests. In summary, this study aims to develop a method for continuously controlling the damping ratio of SA-EMSIS to achieve the dual objectives of addressing both near-fault and far-field ground motions. The seismic isolation performance of the system is validated through shaking table experiments.

SEMI-ACTIVE ELECTROMAGNETIC SEISMIC ISOLATION SYSTEM (SA-EMSIS)

Physical Model of the SA-EMSIS

Figure 1 illustrates the physical model of the Semi-Active Electromagnetic Seismic Isolation System (SA-EMSIS). The SA-EMSIS is composed of a sliding isolation platform, an electromagnetic damper, and a resistance controllable module, designed for seismic isolation applications in equipment protection. The sliding isolation platform, comprising a linear guide rail and a spring, provides foundational support and stability for the SA-EMSIS. The guide rail minimizes friction, while the spring contributes to restoring force, facilitating effective seismic isolation. The electromagnetic damper comprises a rack and pinion assembly, a gearbox, and a rotating DC motor, all of which are mounted on the isolation platform. Additionally, the resistance-controllable module is a critical component for controlling the damping ratio of the isolation system. This module enables real-time adjustment of the external resistance of the SA-EMSIS, thereby modifying its damping ratio.

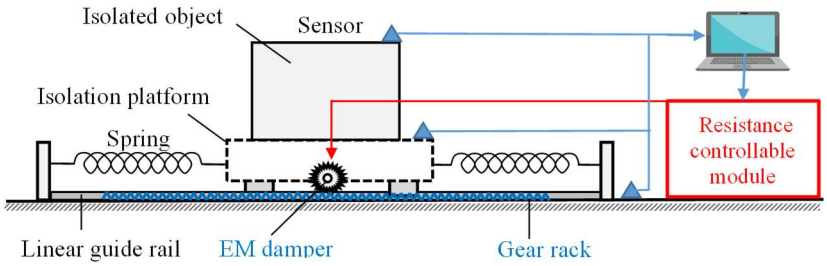

Figure 1. Physical model of the semi-active electromagnetic seismic isolation system.

Prototype of the SA-EMSIS

The prototype of the SA-EMSIS is shown in Figure 2. The controllability of its damping has been verified in a previous study (Lin et al. (2025b)). This research focuses on the design of the SA-EMSIS controller (continuous damping ratio control) to meet the seismic isolation damping requirements for both near-fault and far-field ground motions. As shown in Figure 2(a), the experimental setup uses a rigid mass block as the isolated object. The total mass, comprising the mass block and the isolation platform, is 488.2 kg. Table 1 lists the relevant parameters of the SA-EMSIS prototype. The isolation frequency is 0.35 Hz, the friction coefficient is 0.008, and the inertance is primarily generated by the rotation of the motor's internal rotor. The relationship between the total damping ratio of the SA-EMSIS and the resistance value is as follows:

$$\zeta_b = \frac{20.553}{R_{load}} + 0.0773 \quad (1)$$

The damping ratio (ζ_b) is inversely proportional to the resistance value (R_{load}). The inverse relationship in Eq. (1) enables real-time adjustments of the damping ratio to seismic demands by modifying the resistance value. Figure 2(b) shows the prototype of the resistance-controllable module, which consists of a servo motor, a rotary potentiometer, and a variable resistor. The operating principle involves the servo motor driving the variable resistor through rotational motion to achieve controllability of the resistance value. The potentiometer measures changes in the rotation angle. Based on experimental calibration data, the regression formula relating the rotation angle to the resistance value is as follows:

$$R_{load} = -(1.82 \cdot Angle) + 499.5 \quad (2)$$

Here, R_{load} represents the resistance value of the variable resistor, and $Angle$ denotes the rotation angle of the resistance-controllable module.

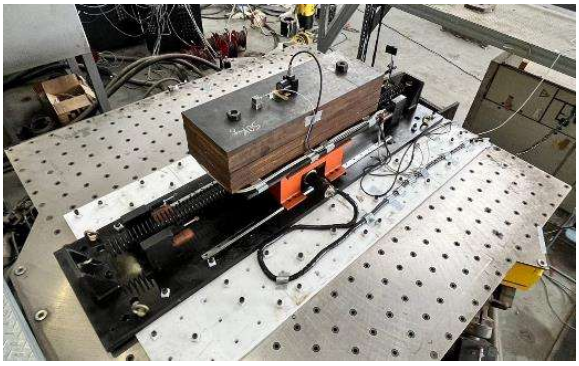

(a) Electromagnetic seismic isolation system

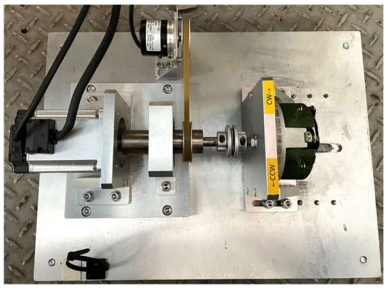

(b) Resistance-controllable module

Figure 2 Prototype of the SA-EMSIS.

THE EQUATION OF MOTION FOR THE SA-EMSIS

Figure 3 illustrates the mathematical model of the SA-EMSIS, where the isolated object is assumed to be a single-degree-of-freedom system. In the figure, m_s, c_s, and k_s represent the mass, damping coefficient, and stiffness of the isolated object, respectively. m_b, k_b, and μ denote the mass, spring stiffness, and friction coefficient of the sliding isolation platform. b_s represents the inertance generated by the electromagnetic damper.

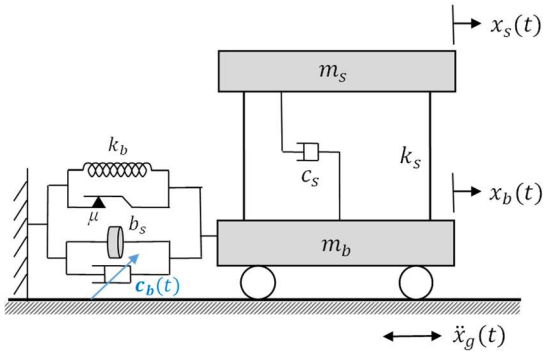

Figure 3 Mathematic model of the SA-EMSIS.

The damping coefficient of the SA-EMSIS, $c_b(t)$ can be expressed as:

$$c_b(t) = 2\sqrt{(m_b + m_s + b_s)k_b}\,\zeta_b(t) \tag{3}$$

The equation of motion for the system shown in Figure 3 can be expressed as:

$$\mathbf{M}\ddot{\boldsymbol{x}}(t) + \mathbf{C}\dot{\boldsymbol{x}}(t) + \mathbf{K}\boldsymbol{x}(t) = -\mathbf{M}'\mathbf{1}\ddot{x}_g(t) - \mathbf{D}(u_b(t) + u_f(t)) \tag{4}$$

Here, u_f represents the frictional force of the sliding isolation platform, and $u_b(t)$, the controllable damping force, can be expressed as:

$$u_b(t) = c_b(t)\dot{x}_b(t) \tag{5}$$

In Eq. (4), the related matrices and vectors are expressed as follows:

$$\boldsymbol{x}(t) = \begin{Bmatrix} x_s(t) \\ x_b(t) \end{Bmatrix}$$

$$\mathbf{M} = \begin{bmatrix} m_s & 0 \\ 0 & m_b + b_s \end{bmatrix},\ \mathbf{C} = \begin{bmatrix} c_s & -c_s \\ -c_s & c_s \end{bmatrix},\ \mathbf{K} = \begin{bmatrix} k_s & -k_s \\ -k_s & k_s + k_b \end{bmatrix}$$

$$\mathbf{M}' = \begin{bmatrix} m_s & 0 \\ 0 & m_b \end{bmatrix},\ \mathbf{1} = \begin{Bmatrix} 1 \\ 1 \end{Bmatrix},\ \mathbf{D} = \begin{Bmatrix} 0 \\ 1 \end{Bmatrix}$$

Here, **M**, **C**, and **K** represent the mass, damping, and stiffness matrices of the entire system, respectively, while $\ddot{x}_g$ denotes the ground acceleration. Notably, the inertance b_s appears in the mass matrix. As shown in Eq. (1), the SA-EMSIS can adjust the external resistance value $R_{load}(t)$ through the resistance controllable module, allowing for the control of the damping ratio $\zeta_b(t)$. Consequently, the damping coefficient $c_b(t)$ becomes a controllable parameter.

HYPERBOLIC TANGENT FUNCTION CONTROLLER

Figure 4 shows the control flow diagram of the SA-EMSIS. When an earthquake induces a response in the system, the displacement signal of the isolation platform, measured by the displacement sensor, is differentiated to obtain the relative velocity ($\dot{x}_b(t)$) of the isolation layer with respect to the ground. This velocity serves as the input to the controller, which determines the damping ratio ($\zeta_b(t)$) of the SA-EMSIS. The determined damping ratio is then converted into the required rotation angle for the resistance controllable module, enabling real-time adjustment of the SA-EMSIS damping ratio.

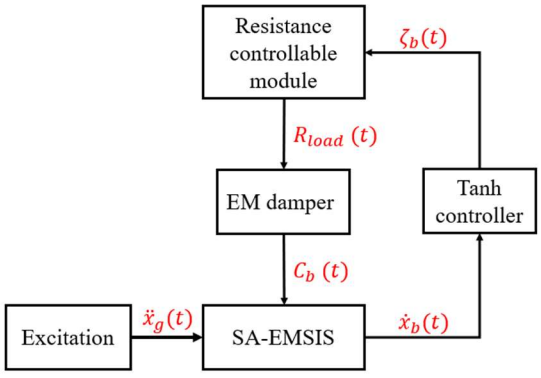

Figure 4 Control flowchart of the SA-EMSIS.

The hyperbolic tangent (*Tanh*) function is used to smooth the control of the damping ratio and can be expressed as follows:

$$\zeta_b(t) = \zeta_{b,max} \cdot Tanh\left(\beta \cdot |\dot{x}_b(t)|\right) \tag{6}$$

Here, $\zeta_{b,max}$=0.34 and β=15 were determined through extensive parametric studies to optimize isolation performance under seismic excitations. Based on the control method in Eq. (6), the relationship between the damping ratio and resistance value in Eq. (1), and the relationship between rotation angle and resistance value in Eq. (2), the actual relationship between the damping ratio and relative velocity for the *Tanh* controller is shown in Figure 5. As observed in the figure, the smooth transition in damping ratio as the relative velocity increases ensures stability during real-time control.

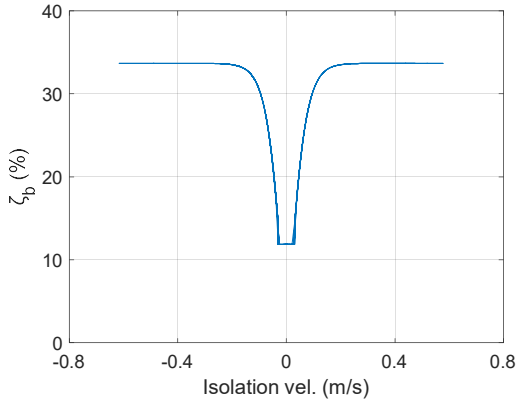

Figure 5 Relationship between damping ratio and isolation velocity.

SHAKING TABLE TEST RESULTS

Figure 2(a) shows a photograph of the SA-EMSIS installed on the shaking table. The parameters of the SA-EMSIS are listed in Table 1. It should be noted that the isolated object in this experiment is a mass block (rigid body), allowing the study to focus on verifying the accuracy of the *Tanh* controller applied in the SA-EMSIS. Additionally, this study selected two ground motion records as input for the shaking table tests: one representing far-field characteristics (Loma Prieta, Hollister) and the other representing strong near-fault characteristics (Chi-Chi, TCU075). These records were chosen based on the classification criteria established by Shahi and Baker (2014).

Table 1 Parameter values of the SA-EMSIS prototype.

Parameter	Values
Total mass ($m_b + m_s$)	(88.2+400)=488.2 kg
Inertance (b_s)	149.5 kg
Stiffness (k_b)	3076.5 N/m
Frequency (f_b)	0.35 Hz
Friction coefficient (μ)	0.008
Total damping ratio (ξ_b)	Controllable

Fitting Between Shaking Table Test Results and Theoretical Simulations

Figure 6 illustrates the fitting between the shaking table test results and theoretical simulations of the SA-EMSIS under the Chi-Chi (TCU075) ground motion. The figure includes various plots: the acceleration of

the isolation layer (subplot a), the displacement of the isolation layer (subplot b), the damping force hysteresis loop (subplot c), the total shear force hysteresis loop of the isolation layer (subplot d), where the vertical axis represents the total shear force calculated by multiplying the measured absolute acceleration ($\ddot{x}_{b,a}$) by the total mass of 488.2 kg, the rotation angle time history of the resistance-controllable module (subplot e), and the total damping ratio time history (subplot f). Due to the stroke limitation of the shaking table, the strong near-fault ground motion Chi-Chi (TCU075) test could only be conducted up to a PGA of 0.15g. The comparison between theoretical and experimental results shown in Figure 6 indicates that the theoretical model of the SA-EMSIS accurately simulates the shaking table test results, thereby verifying the accuracy of both the theoretical analysis and the experimental setup.

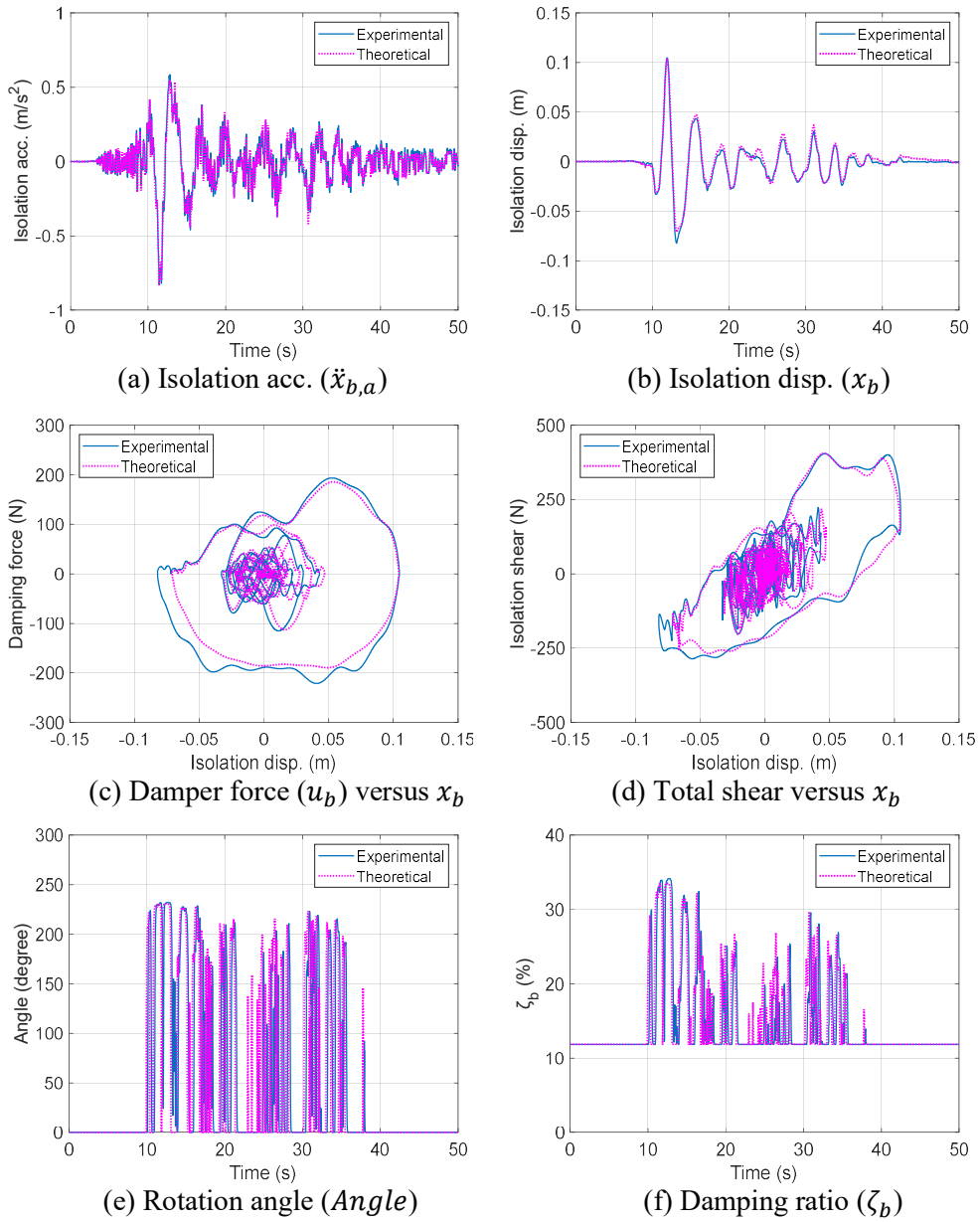

(a) Isolation acc. ($\ddot{x}_{b,a}$) (b) Isolation disp. (x_b)

(c) Damper force (u_b) versus x_b (d) Total shear versus x_b

(e) Rotation angle ($Angle$) (f) Damping ratio (ζ_b)

Figure 6 Comparison of the theoretical and experimental results (Chi-Chi (TCU075), PGA=0.15g).

Comparison Between Semi-Active and Passive Seismic Isolation Systems

Figure 7 compares the dynamic responses of the system under Chi-Chi (TCU075) ground motion (PGA = 0.15g) using the *Tanh* controller and passive control (ζ_b=12%). The results show that the *Tanh* controller effectively reduces both the displacement and acceleration responses of the isolation layer under strong near-fault ground motions. Figure 8 presents the results under Loma Prieta (Hollister) ground motion (PGA = 0.10g), representing far-field ground motions with low PGA values, which occur more frequently. In this case, the *Tanh* controller does not significantly increase the acceleration response of the isolation layer. In summary, the SA-EMSIS paired with the *Tanh* controller achieves more comprehensive seismic isolation performance compared to passive isolation systems.

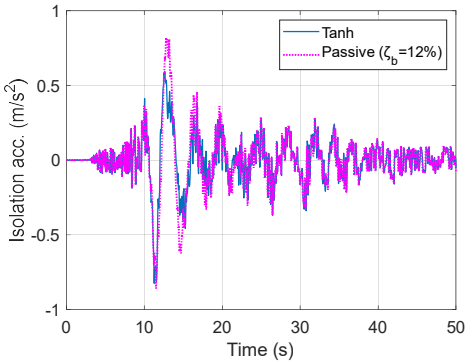

(a) Isolation acc. ($\ddot{x}_{b,a}$)

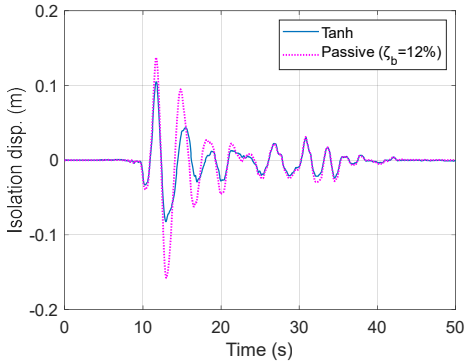

(b) Isolation disp. (x_b)

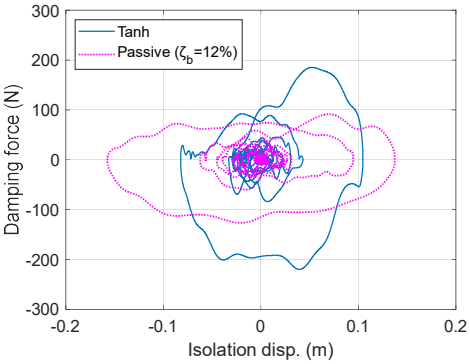

(c) Damper force (u_b) versus x_b

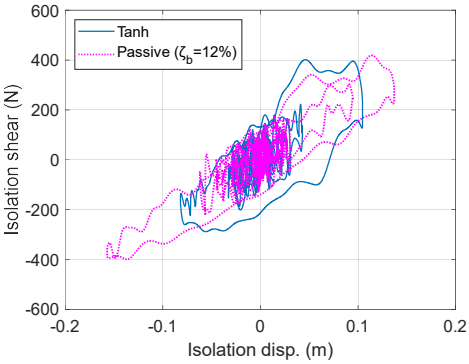

(d) Total shear versus x_b

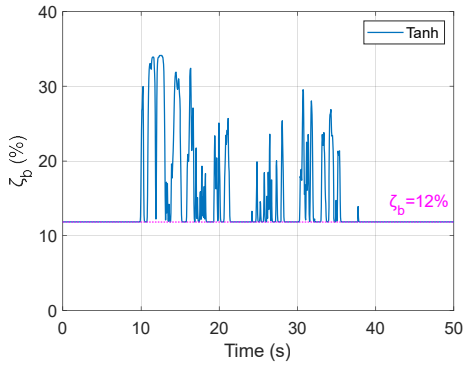

(e) Damping ratio (ζ_b)

Figure 7 Comparison of *Tanh* control and passive control ($\zeta_b = 12\%$) experimental results (Chi-Chi (TCU075), PGA=0.15g).

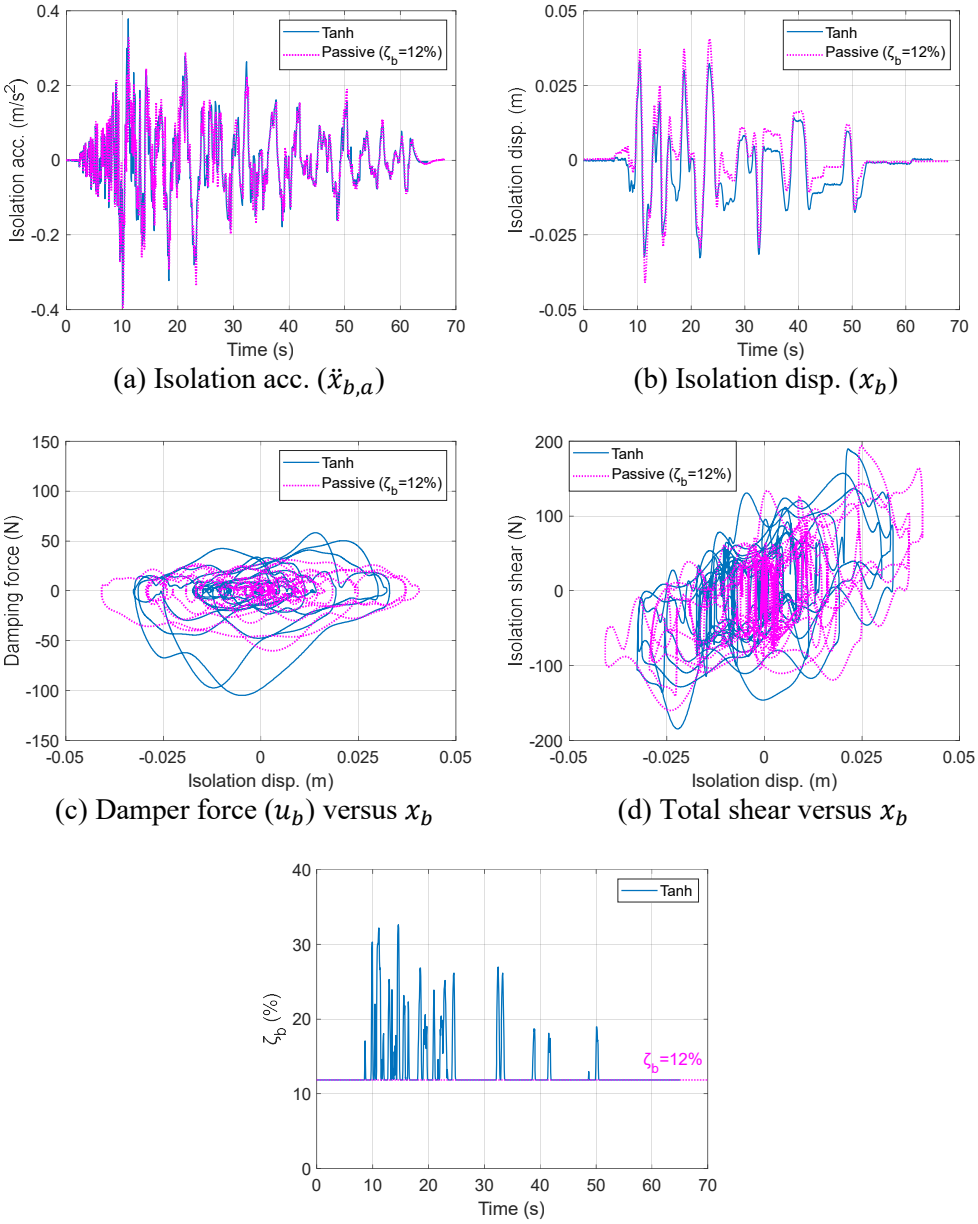

(a) Isolation acc. ($\ddot{x}_{b,a}$) (b) Isolation disp. (x_b)

(c) Damper force (u_b) versus x_b (d) Total shear versus x_b

(e) Damping ratio (ζ_b)

Figure 8 Comparison of *Tanh* control and passive control ($\zeta_b = 12\%$) experimental results (Loma Prieta (Hollister)), PGA=0.1g).

CONCLUSION

To simultaneously meet the seismic isolation requirements under both near-field and far-field ground motions, this study develops the Semi-Active Electromagnetic Seismic Isolation System (SA-EMSIS) and designs a *Tanh* controller. The SA-EMSIS effectively addresses the dual challenges of seismic isolation by maintaining superior acceleration isolation under far-field ground motions and significantly mitigating maximum displacement under near-fault conditions. This dual performance capability demonstrates its potential for real-world applications in critical infrastructure protection. To validate the seismic isolation performance of the SA-EMSIS, shaking table experiments were conducted on the SA-EMSIS prototype

under both far-field and near-fault ground motions. The results show good consistency between the theoretical simulations and experimental dynamic responses, confirming the accuracy of the theoretical model and the shaking table tests. Further comparisons between the SA-EMSIS and passive isolation systems reveal that the SA-EMSIS effectively reduces isolation layer displacement and acceleration under the strong near-fault ground motion, and without increasing acceleration under the far-field ground motion, delivering superior and well-rounded seismic isolation performance. Considering these advantages, the SA-EMSIS offers great potential for deployment in critical infrastructure, including nuclear facilities.

ACKNOWLEDGMENTS

This study received partial funding from the National Science and Technology Council of the Republic of China (Taiwan) under Grant No. NSTC 113-2625-M-992-001.

REFERENCES

Cai, Q., Zhu, S. (2019). "Enhancing the performance of electromagnetic damper cum energy harvester using microcontroller: Concept and experiment validation," *Mechanical Systems and Signal Processing*, 134, 106339.

He, W. L., Agrawal, A. K. (2008). "Analytical model of ground motion pulses for the design and assessment of seismic protective systems," *Journal of Structural Engineering*, 134(7), 1177-1188.

Li, J. Y., Zhu, S. (2021). "Tunable electromagnetic damper with synthetic impedance and self-powered functions," *Mechanical Systems and Signal Processing*, 159, 107822.

Lin, G. L., Lin, C. C., Li, Y. H., Lin, T. T. (2022). "Theoretical and experimental analysis of an electromagnetic seismic isolation system," *Engineering Structures*, 250, 113411.

Lin, G. L., Chang, C. C., Lin, C. S., Lin, C. C., Lin, T. T., Li, Y. H. (2025a). "Experimental investigation of an electromagnetic seismic isolation system with different configurations of inertance," *Journal of Sound and Vibration*, 595, 118698.

Lin, G. L., Chang, M. B., Lin, J. Z. (2025b). "Development of a novel semi-active electromagnetic seismic isolation system," *Engineering Structures*, 333, 120200.

Lu, L. Y., Lin, C. C., Lin, G. L. (2013). "Experimental evaluation of supplemental viscous damping for a sliding isolation system under pulse-like base excitations," *Journal of Sound and Vibration*, 332(8), 1982-1999.

Makris, N., Vassiliou, M. F. (2011). "The existence of 'complete similarities' in the response of seismic isolated structures subjected to pulse-like ground motions and their implications in analysis," *Earthquake Engineering and Structural Dynamics*, 40, 1103-1121.

Naeim, F., Kelly, J. M. (1999). *Design of seismic isolated structures: from theory to practice*, John Wiley & Sons.

Palomera-Arias, R. (2005). "*Passive electromagnetic damping device for motion control of building structures*," Ph.D. Dissertation, Massachusetts Institute of Technology, USA.

Shahi, S. K., Baker, J. W. (2014). "An efficient algorithm to identify strong-velocity pulses in multicomponent ground motions," *Bulletin of the Seismological Society of America*, 104(5), 2456-2466.

Sun, R., Wong, W., Cheng, L. (2023). "Bi-objective optimal design of an electromagnetic shunt damper for energy harvesting and vibration control," *Mechanical Systems and Signal Processing*, 182, 109571.

Tai, W. C., Zuo, L. (2017). "On optimization of energy harvesting from base-excited vibration," *Journal of Sound and Vibration*, 411, 47-59.